ACS APPLIED MATERIALS & INTERFACES

Research Article

www.acsami.org

Quantum Capacitance Based Amplified Graphene Phononics for Studying Neurodegenerative Diseases

Bijentimala Keisham,[⊥,†] Akop Seksenyan,[⊥,‡,§] Steven Denyer,[§] Pouyan Kheirkhah,[§] Gregory D. Arnone,[§] Pablo Avalos,[∥] Abhiraj D. Bhimani,[§] Clive Svendsen,[∥] Vikas Berry,*[,†] and Ankit I. Mehta*[,§]

[†]Department of Chemical Engineering, University of Illinois at Chicago, Chicago 60607, Illinois, United States

[§]Department of Neurosurgery, University of Illinois at Chicago, Chicago 60612, Illinois, United States

[‡]Chicago Medical School, Rosalind Franklin University of Medicine and Science, North Chicago 60064, Illinois, United States

[∥]Regenerative Medicine Institute, Cedars-Sinai Medical Center, Los Angeles 90048, California, United States

Supporting Information

ABSTRACT: Amyotrophic lateral sclerosis (ALS) is the most common adult-onset motor neuron disease (MND) characterized by a rapid loss of upper and lower motor neurons resulting in patient death from respiratory failure within 3−5 years of initial symptom onset. Although at least 30 genes of major effect have been reported, the pathobiology of ALS is not well understood. Compounding this is the lack of a reliable laboratory test which can accurately diagnose this rapidly deteriorating disease. Herein, we report on the phonon vibration energies of graphene as a sensitive measure of the composite dipole moment of the interfaced cerebrospinal fluid (CSF) that includes a signature-composition specific to the patients with ALS disease. The second-order overtone of in-plane phonon vibration energy (2D peak) of graphene shifts by 3.2 ± 0.5 cm^{-1} for all ALS patients studied in this work. Further, the amount of n-doping-induced shift in the phonon energy of graphene, interfaced with CSF, is specific to the investigated neurodegenerative disease (ALS, multiple sclerosis, and MND). By removing a severe roadblock in disease detection, this technology can be applied to study diagnostic biomarkers for researchers developing therapeutics and clinicians initiating treatments for neurodegenerative diseases.

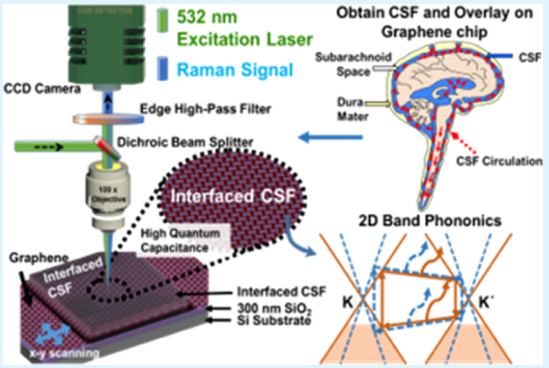

KEYWORDS: *graphene, neurodegenerative disease, Raman, ALS, phonons, detection*

INTRODUCTION

Amyotrophic lateral sclerosis (ALS) is an adult-onset neurodegenerative disease characterized by a rapid loss of motor neurons controlling skeletal muscles.[1] The pathological and molecular features of ALS include mitochondrial dysfunction, increased oxidative stress, detrimental immune activation, and break down of the blood−brain barrier.[2,3] These pathological mechanisms have been previously shown to be reflected in the cerebrospinal fluid (CSF) of both human patients and animal models with ALS.[4,5] Although proteomic and genomic studies of CSF from ALS patients have shown unique differences reflecting the pathophysiology of the disease, currently, there are no reliable biomarkers which can accurately diagnose and monitor the progression of this rapidly deteriorating disease.[6,7] Moreover, patients with monomelic amyotrophy, primary lateral sclerosis, and cervical myelopathy are sometimes misdiagnosed as having ALS and vice versa. Although these diseases manifest with similar clinical motor neuron symptoms, ALS patients have a significantly different and more rapid disease course.[8−10] Given the clinical heterogeneity of ALS, having a disease biomarker will be important for clinicians initiating treatments and basic scientists studying the pathophysiology of the disease. More importantly, a biomarker will be of utmost importance in helping with patient selection when designing therapeutic clinical trials.

Graphene, a two-dimensional (2D) sheet with a honeycomb lattice comprising sp^2-hybridized carbon atoms,[11−15] possesses an ultrasensitive surface with a detection resolution of a single molecule.[16,17] The phononic properties of single-atom-thick graphene are influenced by the dipole potential of any biomaterial or biomolecule interfaced on its surface.[16,18] When graphene comes in contact with the molecules within CSF, the dipole of the interfaced molecules induce an electric field.[19] Because of the large quantum capacitance (sensitivity to be doped by an electric field) of graphene, the dipolar field from the expressed molecular species dopes graphene with electron or hole carriers.[20] This altered density of state affects the vibrational energies of graphene,[16,18,21] which can be mapped using Raman spectroscopy.[22,23] It has been previously established that the Raman peak positions of graphene changes

Received: September 12, 2018
Accepted: November 23, 2018
Published: November 23, 2018

DOI: 10.1021/acsami.8b15893
ACS Appl. Mater. Interfaces XXXX, XXX, XXX−XXX

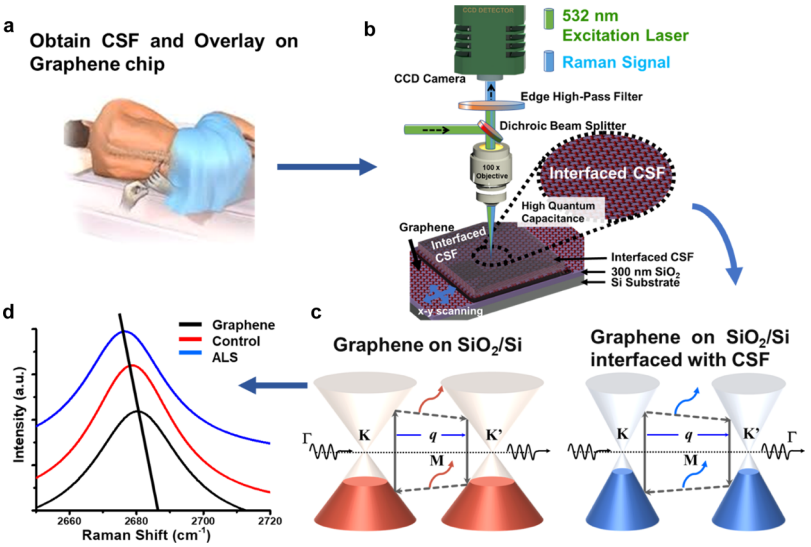

Figure 1. Interfaced CSF induces n-doping of graphene. (a) Graphic representation of obtaining CSF via lumbar puncture. (b) Schematic depicting the setup of graphene-based detection of ALS using Raman spectroscopy. Composite dipole moment of CSF coupled with the high quantum capacitance of graphene sensitively modifies the 2D band phononics. (c) Graphical depiction of Dirac energy barrier alterations in the presence of human CSF, with wave vector q, Brillouin zone center Γ, M points in the middle of the hexagonal sides, and K and K' points representing the corners of the hexagons. (d) 2D Raman peak of graphene in the presence of control and ALS CSF samples.

Table 1. Demographic and Clinical Characteristics of Subjects Included in This Study

sample	age	gender	clinical diagnosis	neuropathological diagnosis	clinical and pathological features
control	57	M	heart disease	n/a	cytomegalovirus inclusion body disease, renal failure
	59	M	cancer (esophageal)	n/a	n/a
	59	M	pulmonary embolism	normal	arthritis
	65	F	cancer (lung)	n/a	n/a
	72	M	pulmonary embolism	n/a	n/a
	84	F	cancer (unknown)	n/a	n/a
	101	F	cancer (colon)	n/a	hypertension, osteoporosis
ALS	32	M	ALS	ALS	n/a
	45	M	ALS	ALS	n/a
	50	M	ALS	ALS	recent hypoxic changes in the cerebrum
	52	F	ALS	clinical diagnosis only	n/a
	58	F	ALS	ALS	n/a
	58	M	ALS	clinical diagnosis only	depression
	66	F	ALS	ALS	polyneuritis
	66	M	ALS	ALS	cancer (unknown)
	68	M	ALS	ALS	n/a
	70	M	ALS	ALS	diabetes mellitus, hypertension
	70	M	ALS	ALS	recent hypoxic changes in the cerebrum
	74	F	ALS	ALS	n/a
	76	F	ALS	ALS	moderate cerebral atherosclerosis
MS	64	F	secondary progressive MS	n/a	n/a
	79	F	secondary progressive MS	n/a	n/a
	81	M	secondary progressive MS	n/a	n/a
MND	52	M	MND	n/a	n/a
	60	M	MND	n/a	dementia
	67	M	MND	n/a	n/a

with the concentration of carriers injected in the lattice.[24] Specifically, the 2D peak position observed between 2600 and 2700 cm^{-1} decreases with n-doping (electron) and increases with p-doping (hole), unlike the G peak whose position increases with either type of doping (Kohn anomaly for Raman-active G band).[25−28] Further, the G peak position gets saturated with increasing doping as doping leads to non-adiabatic removal of G-phonon dispersion. Hence, the 2D peak provides comprehensive information regarding the polarity as well as the density of injected charge carriers.[24,29,30] Further, it is important to note that the sensitive platform provided by graphene cannot be expected from graphene oxide, as the latter suffers from heavy and inconsistent lattice disorders, with relatively weak 2D Raman signals (prominent D and G peaks), because of the presence of many defects and oxygen functional groups.[31−35]

DOI: 10.1021/acsami.8b15893
ACS Appl. Mater. Interfaces XXXX, XXX, XXX−XXX

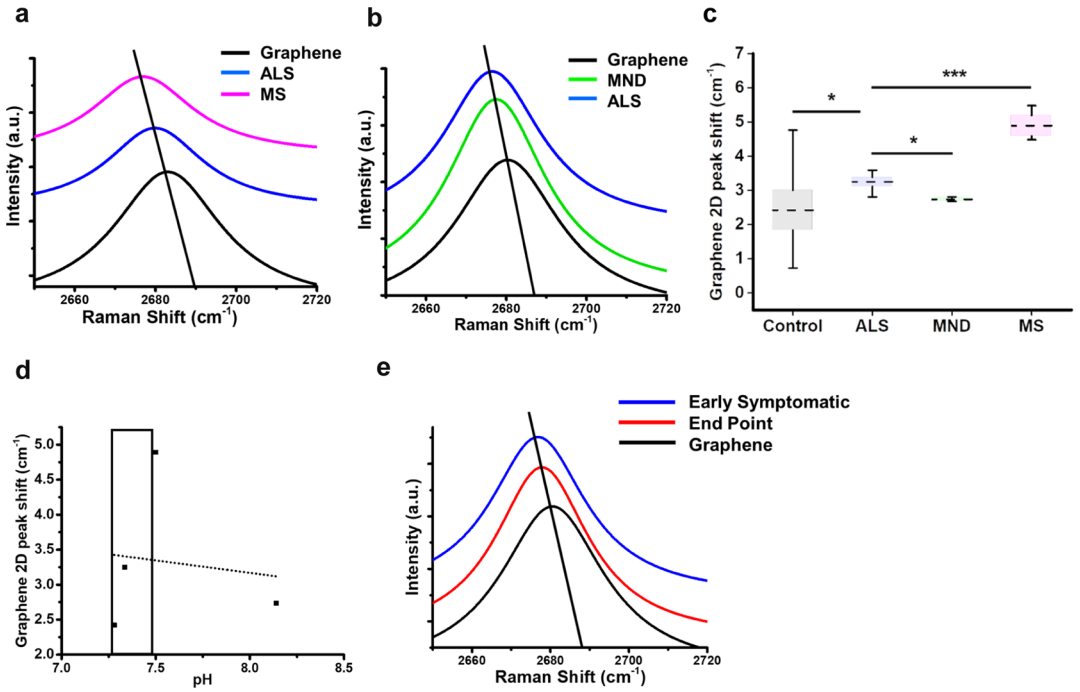

Figure 2. n-Doping of graphene by CSF from neurodegenerative diseases. (a) Relative to ALS, 2D peak changes of MS (n = 3) and (b) MND (n = 3). (c) Quantification of 2D peak shift by human CSF samples. (d) Human CSF samples for each group were pooled and pH was measured, demonstrating no correlation between pH and 2D peak shifts (box indicates normal physiologic pH range). (e) $SOD1^{G93A}$ transgenic rat CSF samples taken at ES (n = 2) and EP (n = 4) subjected to Raman spectroscopy. Error bars, outliers; box, standard error of the mean; dashed line, mean; $^*P < 0.05$, $^{**}P < 0.01$, $^{***}P < 0.001$, Student's t-test.

Previously, we applied this ultrasensitive property of graphene to differentiate human glioma cells from human astrocytes.[20] Extrapolating from these findings, we monitored the phononic properties of CSF-interfaced graphene to study the effectiveness of this tool in differentiating ALS from other neurodegenerative diseases.

EXPERIMENTAL SECTION

Postmortem human CSF samples were obtained from the Human Brain and Spinal Fluid Resource Center, which is sponsored by NINDS/NIMH, National Multiple Sclerosis Society and Department of Veterans Affairs. CSF samples were collected from patients with ALS, multiple sclerosis (MS), motor neuron diseases (MNDs), and control subjects. The CSF was then interfaced with graphene produced by chemical vapor deposition and transferred onto the SiO_2/Si substrate, with a coverslip on top to reduce evaporation. The graphene–CSF system was then characterized using Raman spectroscopy, with a laser wavelength of 532 nm. A similar protocol was followed for analyzing the CSF from $SOD1^{G93A}$ transgenic rat model of ALS, at two distinct disease stages—early symptomatic (ES) and end point (EP). The experimental steps are explained in detail in the Supporting Information, Section S1.

RESULTS AND DISCUSSION

Doping Effect of CSF on Graphene. We first tested whether human CSF (Figure 1a) will have any influence on the phononic properties of graphene. Using a previously published protocol from our own laboratory,[20] graphene on the SiO_2/Si substrate was interfaced with 30 μL of CSF from postmortem control subjects (non-neurological causes of death) (Table 1) and studied under Raman spectroscopy (area of analysis ≈ 0.5 μm^2) (Figure 1b). We focused our spectral analysis on the second-order overtone of in-plane phonon vibration energies (2D peak) of graphene, as this peak has been previously established to be altered distinctly by the concentration of different carrier types injected in the lattice.[24] Relative to pristine graphene, we found that control CSF samples induced a slight, but significant, n-doping effect and a red shift of ∼1.2–2.4 cm^{-1} in the 2D peak of the Raman spectra (Figure 1d). These results point to the existence of dopants in the control CSF. The presence of any dopants changes the properties of graphene, including the electrical and phononic attributes. Analyzing the electronic band structure of graphene is an effective approach to interpret the effects of doping,[36,37] which can be achieved by examining the shape of the Dirac cones of graphene.[36,38] Graphene on SiO_2/Si is p-doped, which modifies the resonance conditions of the 2D phonons and hence renormalizing the electronic bands.[39] This renormalization pushes the electronic bands away from the K and K' points (Figure 1c), thereby increasing the corresponding 2D mode energy. When the CSF is interfaced with graphene, it n-dopes the graphene lattice. The resulting n-doping renormalizes the electronic bands again, which in turn shifts them toward the K and K' points reducing the 2D energy (Figure 1c). These alterations in graphene phononics are an indication that components in the CSF cause meaningful and measurable changes, which can be monitored using Raman spectroscopy.

Specific Effects of Different Neurodegenerative Diseases on the Phonon Vibration Energies of Graphene. Once we established that human CSF has detectable influence on the phononic properties of graphene, we investigated whether this measured effect can be used to distinguish ALS from other neurodegenerative diseases, namely, MS and other MNDs. Even though these diseases affect the central nervous system (CNS), driving pathological processes are widely different.[8] We hypothesized that the disease-specific components in CSF will interact differently

DOI: 10.1021/acsami.8b15893
ACS Appl. Mater. Interfaces XXXX, XXX, XXX–XXX

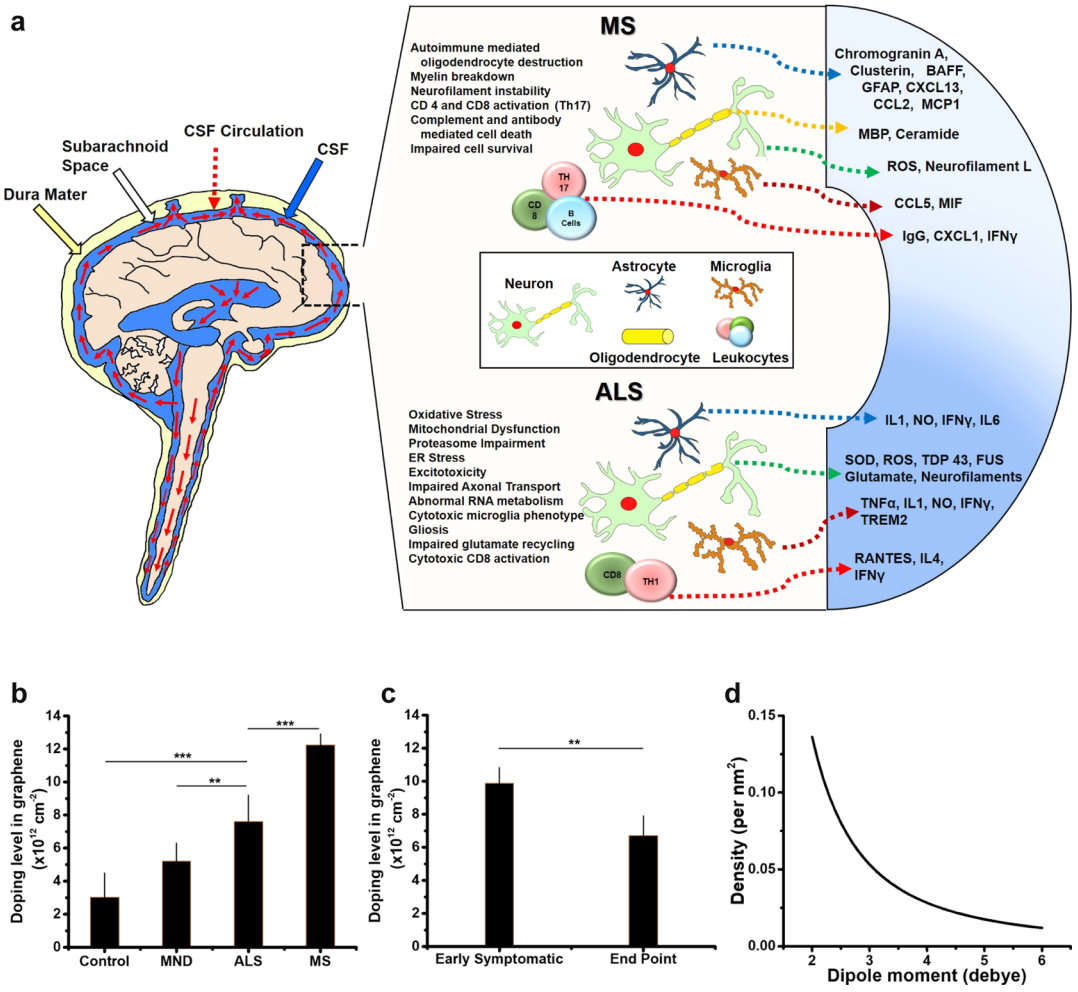

Figure 3. Carrier concentrations of graphene interfaced with CSF. (a) Flow of CSF in CNS and the previously reported secreted factors found in the CSF of MS and ALS patients. (b) Calculated graphene carrier concentration in the presence of human and (c) $SOD1^{G93A}$ rat CSF samples. (d) Calculated average induced dipole moment of human ALS CSF samples. Error bar, standard error of the mean; $*P < 0.05$, $**P < 0.01$, $***P < 0.001$, Student's *t*-test.

with graphene and therefore change its properties in a disease-specific manner.

We first tested the postmortem CSF samples from 13 ALS patients, 11 of which had pathologically corroborating diagnosis of the disease in addition to clinical findings (Table 1). In these groups of patients, we found the shift of Raman 2D peak to be more pronounced (~3−3.5 cm^{-1}) (Figure 1d), indicating a higher n-doping of graphene. This difference between the controls and ALS patients is possibly related to the underlying neuroinflammation, metabolic alteration, and increased production of reactive oxygen species (ROS) in ALS patients.[3,40−42] Subsequently, we tested three CSF samples from patients who were diagnosed with secondary progressive MS and three samples from MND patients, who had a form of motor neuron pathology that is not ALS. Interfacing the CSF of MS and MND patients demonstrated a marked difference in the extent of graphene doping compared to ALS and control samples (Figure 2a−c). These findings suggest that the disease-related changes in CSF have a pronounced effect on the doping of graphene and the degree of doping is related to the underlying disease. To rule out the possibility that these changes were mainly due to alterations in pH, as this has been previously shown to influence the doping of graphene,[43] we measured the pH of pooled CSF samples. Interestingly, we found no significant correlation between pH and the amount of n-doping (Figure 2d). This argues for the hypothesis that other disease-specific factors (cytokines, ROS, and lipids) in CSF, with different dipole moments, are the main reason for the observed differences among the disease group.

These results motivated us to investigate whether the alteration in the doping level of graphene changes with the disease course. For this purpose, we studied CSF from $SOD1^{G93A}$ transgenic rat model generated by forced over-expression of the mutated human SOD1 protein.[44] The mutations in the SOD1 gene, specifically the G93A amino acid alteration, have been well established as one of the causes of ALS.[8] Thus, overexpression of the mutated protein reproduces many of the pathological features of human ALS. More importantly, this rat model has been previously characterized and the clinical stages correlated with the neuropathological severity.[45] As such, this allowed us to test whether the measured doping in graphene from human CSF is also present in the rat and whether the amount of doping can be used to monitor the progression of the disease. The CSF samples from rats at the ES and the EP stages of the disease were tested. Crudely, the ES stage is comparable to the time point at which human patients generally first present to the clinic with

DOI: 10.1021/acsami.8b15893
ACS Appl. Mater. Interfaces XXXX, XXX, XXX−XXX

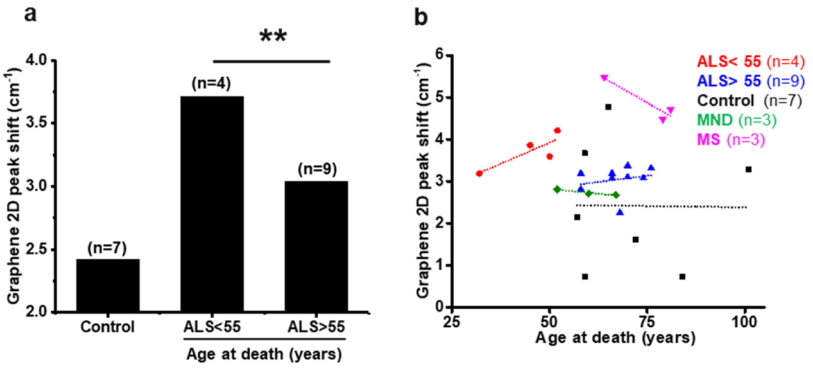

Figure 4. Age of ALS patients correlates with the amount of graphene 2D peak shift. (a) Amount of 2D peak shift was compared among ALS patients after stratifying them into two age groups at the time of death [<55 years old (n = 4) and >55 years old (n = 9), with 55 years of age being the average age of ALS diagnosis]. Comparing these two ALS age groups gave a statistically significant difference with a P-value of 0.006. (b) Age at death of all the study samples was graphed against the amount of 2D peak shift to look for possible correlation between these two parameters. Both ALS age groups demonstrated a positive correlation with age (red and blue lines), whereas the other two diseases had a negative correlation (green and purple lines), and the control samples (black line) had no correlation with age.

neurological symptoms. Results from these experiments showed significantly enhanced doping in both animal groups, with the ES rats exhibiting a much higher shift in the vibrational energy of the 2D band of graphene (Figure 2e).

Alteration of Carrier Concentration of Graphene by Interfaced CSF. The ultrasensitivity of graphene to any kind of doping stems from its high quantum capacitance, given by $C_Q = \frac{4e^2\sqrt{\pi}}{h\vartheta_F}\sqrt{n_R}$, where e is the charge of electron, h is Planck's constant, ϑ_F is the Fermi velocity of the Dirac electron, and n_R is the total carrier concentration of graphene.[46] The phononic properties of graphene modified by doping are monitored via Raman spectroscopy through which the carrier concentration of graphene can be determined.[24] Here, the intrinsic concentration of graphene and carrier doping, via the components of CSF, comprise the total carrier concentration of graphene. Previous studies have demonstrated that the CSF of ALS and MS patients contain different concentrations and types of secreted factors, such as cytokines, lipids, and ROS (Figure 3a). Therefore, we hypothesized that the dipole moment of these CSF factors will enhance the effective electrical field of graphene,[32,46−48] essentially doping the graphene lattice via quantum coupling and modifying its carrier concentration, in a disease-specific manner. Calculating the total carrier concentration of CSF-interfaced graphene demonstrated a clear distinction between ALS and other diseases (Figure 3b). Similar calculations done on rat CSF samples demonstrated a statistically significant difference (Figure 3c). Because the concentration of these proteins, lipids, nucleic acids, and ROS are also expected to be different in these diseases and vary across the graphene surface, a range of average dipole moments and density of these molecules were also calculated (Figures 3d, S1, and S2). These results suggest that the change in the carrier concentration of graphene can be attributed to the varying dipole moments of the CSF components.

Correlation of the Age of ALS Patients with Varying Levels of Vibrational Energies of Graphene. Our experimental results, along with carrier concentration calculations, strongly support the hypothesis that biological factors in CSF have a direct influence on graphene phononics and that any difference in their quantity can be detected by Raman spectroscopy. This motivated us to investigate whether there are any graphene doping differences among ALS patients and if such differences correlated with demographic parameters. We noticed that ALS patients clustered into two distinct groups based on age. Patients below the age of 55, interestingly, this being the average age at diagnosis, had statistically higher 2D shifts compared to patients above the age of 55 (Figure 4a). It is well documented that patients diagnosed before the age of 55 generally have the familial form ALS, whereas older patients tend to be more of the sporadic type. In support of this observation, two out of the three patients who had documented a family history of ALS fell into the "younger" (<55 years of age) patient group whereas three out of three sporadic patients fell into the "older" (>55 years of age) group. Moreover, out of all the disease groups in our study, only ALS patients tended to have a positive correlation with age (Figure 4b). The other diseases displayed a negative correlation, and the control samples had no correlation with age, suggesting that the biology of these different diseases is being captured by graphene and reflected in the alteration of its phononic properties.

CONCLUSIONS

The development of a disease biomarker for ALS has been challenging.[8,9] Various strategies, including mass spectroscopy and large-scale sequencing, have been employed with limited success thus far.[9] Here, the ultrasensitive property of graphene was used to study the CSF of ALS patients and disease controls as a novel approach to a possible disease biomarker. We found that the interaction of CSF with graphene causes significant changes in its vibrational energies, which can be measured using Raman spectroscopy. Our findings of the measured differences between ALS and MND offer a unique strategy to develop a diagnostic biomarker that can be used to distinguish ALS from other forms of MNDs. Moreover, the differences in the density curves reflect the disease-specific composition of the biomolecules, with varying dipole moments, found in each of the neurodegenerative diseases. These results indicate that graphene is able to sense even the slight variations of the concentration of biological species that are potentially contributing to the specificity of each disease. Even with the limited sample size, it is tempting to speculate that the alterations in graphene are a reflection of the underlying biology and that the amount of n-doping is potentially

DOI: 10.1021/acsami.8b15893
ACS Appl. Mater. Interfaces XXXX, XXX, XXX−XXX

stratifying the ALS patients into biologically distinct groups. In combination with the results from rat studies, we believe that these findings raise the exciting possibility that graphene can be eventually used to stratify ALS patients into distinct clinical and biological groups. These results can have profound clinical implications and applications.

In summary, we demonstrate a robust system to investigate ALS by using graphene. The second-order overtone of in-plane vibration of graphene provides an ultrasensitive platform to study the interface of CSF and graphene. It is important to note that this strategy does not analyze the Raman signal of CSF; rather, it looks at the change in the Raman signal from interfaced graphene. On the basis of our analysis, it can be concluded that this ultrasensitive platform can efficaciously differentiate neurodegenerative diseases. Although the exact causes for these differences are beyond the scope of this study, we hypothesize that the composite effect of inflammatory molecules, ROS, and other bioactive substances that have been previously demonstrated in ALS is the contributing factor for the measured changes in the properties of graphene.[49] Further, monitoring the progression of ALS has always been challenging and understanding this process is critical in the fight against this disease. Our results from the SOD1^{G93A} transgenic rat model argue for the ability to use the measured changes in the 2D peak of graphene to monitor the progression of the disease. These results suggest that our graphene platform cannot only be used to potentially diagnose ALS, but also to monitor its progression and, in the future, to study the efficacy of therapeutics. A prospective study will be needed to test whether our findings correlate with more extensive clinical parameters and whether it can stratify patients into distinct subgroups, as suggested by Appel et al.[49] Even with the limitations of our study, the initial results offer an unprecedented phononic mechanism in graphene to study human CSF for the diagnosis of neurodegenerative diseases.

■ ASSOCIATED CONTENT

Supporting Information

The Supporting Information is available free of charge on the ACS Publications website at DOI: 10.1021/acsami.8b15893.

Experimental methods and average dipole moment comparison for different sample groups (PDF)

■ AUTHOR INFORMATION

Corresponding Authors

*E-mail: vikasb@uic.edu (V.B.).

*E-mail: ankitm@uic.edu (A.I.M.).

ORCID

Vikas Berry: 0000-0002-1102-1996

Author Contributions

⊥B.K. and A.S. are co-first authors. These authors contributed equally to this work. A.S. conceived the idea of using the detection technology developed by V.B., A.I.M., and B.K. for ALS detection. B.K., A.S., C.S., V.B., and A.I.M. designed the experiments. B.K. fabricated the graphene detection system and performed the detection experiments. A.S., S.D., P.K., G.D.A., and A.D.B. contributed in obtaining the CSF samples. B.K. and A.S. analyzed the Raman data and made the figures in the manuscript. P.A. and C.S. developed and characterized the transgenic rat model and provided the CSF samples from this model. B.K., A.S., V.B., and A.I.M. wrote the manuscript. All authors contributed to the discussion, analysis, and interpretation of the results and reviewed the manuscript. All authors have given approval to the final version of the manuscript.

Funding

The authors acknowledge the financial support from ONR (N00014-18-1-2583), NSF (CMMI-1503681), and the University of Illinois at Chicago (Seed Grant). A.S. is a recipient of the AANS-NREF summer research fellowship for this project.

Notes

The authors declare no competing financial interest.

■ ACKNOWLEDGMENTS

The authors would like to thank Phong Nguyen for useful discussions regarding the calculations of average dipole moments and James S. Riehl for his assistance on human CSF samples.

■ REFERENCES

(1) Talbott, E. O.; Malek, A. M.; Lacomis, D. The Epidemiology of Amyotrophic Lateral Sclerosis. In *Handbook of Clinical Neurology*; Science Direct, 2016; Vol. *138*, pp 225−238.

(2) van Es, M. A.; Hardiman, O.; Chio, A.; Al-Chalabi, A.; Pasterkamp, R. J.; Veldink, J. H.; van den Berg, L. H. Amyotrophic Lateral Sclerosis. *The Lancet* **2017**, *390*, 2084−2098.

(3) Bozzo, F.; Mirra, A.; Carrì, M. T. Oxidative Stress and Mitochondrial Damage in the Pathogenesis of ALS: New Perspectives. *Neurosci. Lett.* **2017**, *636*, 3−8.

(4) Gray, E.; Larkin, J. R.; Claridge, T. D. W.; Talbot, K.; Sibson, N. R.; Turner, M. R. The Longitudinal Cerebrospinal Fluid Metabolomic Profile of Amyotrophic Lateral Sclerosis. *Amyotroph. Lateral Scler. Front. Degener.* **2015**, *16*, 456−463.

(5) Dodge, J. C.; Treleaven, C. M.; Fidler, J. A.; Tamsett, T. J.; Bao, C.; Searles, M.; Taksir, T. V.; Misra, K.; Sidman, R. L.; Cheng, S. H.; et al. Metabolic Signatures of Amyotrophic Lateral Sclerosis Reveal Insights into Disease Pathogenesis. *Proc. Natl. Acad. Sci.* **2013**, *110*, 10812−10817.

(6) Chiò, A.; Traynor, B. J. Biomarkers for ALS-in search of the Promised Land. *Nat. Rev. Neurol.* **2015**, *11*, 72−74.

(7) Tarasiuk, J.; Kułakowska, A.; Drozdowski, W.; Kornhuber, J.; Lewczuk, P. CSF Markers in Amyotrophic Lateral Sclerosis. *J. Neural Trans.* **2012**, *119*, 747−757.

(8) Bäumer, D.; Talbot, K.; Turner, M. R. Advances in Motor Neurone Disease. *J. R. Soc. Med.* **2014**, *107*, 14−21.

(9) Turner, M. R.; Benatar, M. Ensuring Continued Progress in Biomarkers for Amyotrophic Lateral Sclerosis. *Muscle and Nerve* **2015**, *51*, 14−18.

(10) Staff, N. P.; Appel, S. H. The Immune System Continues to Knock at the ALS Door. *Neuromuscular Disorders* **2016**, *26*, 335−336.

(11) Schedin, F.; Geim, A. K.; Morozov, S. V.; Hill, E. W.; Blake, P.; Katsnelson, M. I.; Novoselov, K. S. Detection of Individual Gas Molecules Adsorbed on Graphene. *Nat. Mater.* **2007**, *6*, 652−655.

(12) Mohanty, N.; Berry, V. Graphene-Based Single-Bacterium Resolution Biodevice and DNA Transistor: Interfacing Graphene Derivatives with Nanoscale and Microscale Biocomponents. *Nano Lett.* **2008**, *8*, 4469−4476.

(13) Mohanty, N.; Fahrenholtz, M.; Nagaraja, A.; Boyle, D.; Berry, V. Impermeable Graphenic Encasement of Bacteria. *Nano Lett.* **2011**, *11*, 1270−1275.

(14) Wang, X.; Zhi, L.; Müllen, K. Transparent, Conductive Graphene Electrodes for Dye-Sensitized Solar Cells. *Nano Lett.* **2008**, *8*, 323−327.

(15) Pumera, M. Graphene in Biosensing. *Mater. Today* **2011**, *14*, 308−315.

(16) Geim, A. K.; Novoselov, K. S. The Rise of Graphene. *Nat. Mater.* **2007**, *6*, 183−191.

DOI: 10.1021/acsami.8b15893
ACS Appl. Mater. Interfaces XXXX, XXX, XXX−XXX

(17) Wang, Y.; Li, Z.; Wang, J.; Li, J.; Lin, Y. Graphene and Graphene Oxide: Biofunctionalization and Applications in Biotechnology. *Trends Biotechnol.* **2011**, *29*, 205−212.
(18) Sreeprasad, T. S.; Berry, V. How Do the Electrical Properties of Graphene Change with Its Functionalization? *Small* **2013**, *9*, 341−350.
(19) Deng, S.; Gao, E.; Wang, Y.; Sen, S.; Sreenivasan, S. T.; Behura, S.; Král, P.; Xu, Z.; Berry, V. Confined, Oriented, and Electrically Anisotropic Graphene Wrinkles on Bacteria. *ACS Nano* **2016**, *10*, 8403−8412.
(20) Keisham, B.; Cole, A.; Nguyen, P.; Mehta, A.; Berry, V. Cancer Cell Hyperactivity and Membrane Dipolarity Monitoring via Raman Mapping of Interfaced Graphene: Towards Non-Invasive Cancer Diagnostics. *ACS Appl. Mater. Interfaces* **2016**, *48*, 32717.
(21) Sreeprasad, T. S.; Nguyen, P.; Alshogeathri, A.; Hibbeler, L.; Martinez, F.; McNeil, N.; Berry, V. Graphene Quantum Dots Interfaced with Single Bacterial Spore for Bio-Electromechanical Devices: A Graphene Cytobot. *Sci. Rep.* **2015**, *5*, 9138.
(22) Malard, L. M.; Pimenta, M. A.; Dresselhaus, G.; Dresselhaus, M. S. Raman Spectroscopy in Graphene. *Phys. Rep.* **2009**, *473*, 51−87.
(23) Ferrari, A. C.; Basko, D. M. Raman Spectroscopy as a Versatile Tool for Studying the Properties of Graphene. *Nat. Nanotechnol.* **2013**, *8*, 235−246.
(24) Das, A.; Pisana, S.; Chakraborty, B.; Piscanec, S.; Saha, S. K.; Waghmare, U. V.; Novoselov, K. S.; Krishnamurthy, H. R.; Geim, A. K.; Ferrari, A. C.; et al. Monitoring Dopants by Raman Scattering in an Electrochemically Top-Gated Graphene Transistor. *Nat. Nanotechnol.* **2008**, *3*, 210−215.
(25) Ferrari, A. C. Raman Spectroscopy of Graphene and Graphite: Disorder, Electron-Phonon Coupling, Doping and Nonadiabatic Effects. *Solid State Commun.* **2007**, *143*, 47−57.
(26) Ferrari, A. C.; Meyer, J. C.; Scardaci, V.; Casiraghi, C.; Lazzeri, M.; Mauri, F.; Piscanec, S.; Jiang, D.; Novoselov, K. S.; Roth, S.; et al. Raman Spectrum of Graphene and Graphene Layers. *Phys. Rev. Lett.* **2006**, *97*, 187401.
(27) Casiraghi, C.; Hartschuh, A.; Lidorikis, E.; Qian, H.; Harutyunyan, H.; Gokus, T.; Novoselov, K. S.; Ferrari, A. C. Rayleigh Imaging of Graphene and Graphene Layers. *Nano Lett.* **2007**, *7*, 2711−2717.
(28) Ni, Z.; Wang, Y.; Yu, T.; Shen, Z. Raman Spectroscopy and Imaging of Graphene. *Nano Res.* **2008**, *1*, 273−291.
(29) Basko, D.; Piscanec, S.; Ferrari, A. Electron-Electron Interactions and Doping Dependence of the Two-Phonon Raman Intensity in Graphene. *Phys. Rev. B: Condens. Matter Mater. Phys.* **2009**, *80*, 165413.
(30) Nguyen, P.; Berry, V. Graphene Interfaced with Biological Cells: Opportunities and Challenges. *J. Phys. Chem. Lett.* **2012**, *3*, 1024−1029.
(31) Eda, G.; Fanchini, G.; Chhowalla, M. Large-Area Ultrathin Films of Reduced Graphene Oxide as a Transparent and Flexible Electronic Material. *Nat. Nanotechnol.* **2008**, *3*, 270−274.
(32) Nguyen, P.; Li, J.; Sreeprasad, T. S.; Jasuja, K.; Mohanty, N.; Ikenberry, M.; Hohn, K.; Shenoy, V. B.; Berry, V. Covalent Functionalization of Dipole-Modulating Molecules on Trilayer Graphene: An Avenue for Graphene-Interfaced Molecular Machines. *Small* **2013**, *9*, 3823−3828.
(33) Pope, M. A.; Aksay, I. A. Four-Fold Increase in the Intrinsic Capacitance of Graphene through Functionalization and Lattice Disorder. *J. Phys. Chem. C* **2015**, *119*, 20369−20378.
(34) Akhavan, O. Bacteriorhodopsin as a Superior Substitute for Hydrazine in Chemical Reduction of Single-Layer Graphene Oxide Sheets. *Carbon* **2015**, *81*, 158−166.
(35) Voiry, D.; Yang, J.; Kupferberg, J.; Fullon, R.; Lee, C.; Jeong, H. Y.; Shin, H. S.; Chhowalla, M. High-Quality Graphene via Microwave Reduction of Solution-Exfoliated Graphene Oxide. *Science* **2016**, *353*, 1413−1416.
(36) Elias, D. C.; Gorbachev, R. V.; Mayorov, A. S.; Morozov, S. V.; Zhukov, A. A.; Blake, P.; Ponomarenko, L. A.; Grigorieva, I. V.; Novoselov, K. S.; Guinea, F.; et al. Dirac Cones Reshaped by Interaction Effects in Suspended Graphene. *Nat. Phys.* **2011**, *7*, 701−704.
(37) Sasaki, K. I.; Kato, K.; Tokura, Y.; Suzuki, S.; Sogawa, T. Decay and Frequency Shift of Both Intervalley and Intravalley Phonons in Graphene: Dirac-Cone Migration. *Phys. Rev. B: Condens. Matter Mater. Phys.* **2012**, *86*, 1−6.
(38) Huang, M.; Yan, H.; Heinz, T. F.; Hone, J. Probing Strain-Induced Electronic Structure Change in Graphene by Raman Spectroscopy. *Nano Lett.* **2010**, *10*, 4074−4079.
(39) Li, Y. *Probing the Response of Two-Dimensional Crystals by Optical Spectroscopy*; Springer, 2014; Vols. *9*−*18*.
(40) Al-Chalabi, A.; Hardiman, O.; Kiernan, M. C.; Chiò, A.; Rix-Brooks, B.; van den Berg, L. H. Amyotrophic Lateral Sclerosis: Moving towards a New Classification System. *Lancet Neurol.* **2016**, *15*, 1182−1194.
(41) D'Amico, E.; Factor-Litvak, P.; Santella, R. M.; Mitsumoto, H. Clinical Perspective on Oxidative Stress in Sporadic Amyotrophic Lateral Sclerosis. *Free Radic. Biol. Med.* **2013**, *65*, 509−527.
(42) Hooten, K. G.; Beers, D. R.; Zhao, W.; Appel, S. H. Protective and Toxic Neuroinflammation in Amyotrophic Lateral Sclerosis. *Neurotherapeutics* **2015**, *12*, 364−375.
(43) Paulus, G. L. C.; Nelson, J. T.; Lee, K. Y.; Wang, Q. H.; Reuel, N. F.; Grassbaugh, B. R.; Kruss, S.; Landry, M. P.; Kang, J. W.; Vander Ende, E.; et al. A Graphene-Based Physiometer Array for the Analysis of Single Biological Cells. *Sci. Rep.* **2014**, *4*, 6865.
(44) Howland, D. S.; Liu, J.; She, Y.; Goad, B.; Maragakis, N. J.; Kim, B.; Erickson, J.; Kulik, J.; DeVito, L.; Psaltis, G.; et al. Focal Loss of the Glutamate Transporter EAAT2 in a Transgenic Rat Model of SOD1 Mutant-Mediated Amyotrophic Lateral Sclerosis (ALS). *Proc. Natl. Acad. Sci.* **2002**, *99*, 1604−1609.
(45) Thomsen, G. M.; Gowing, G.; Latter, J.; Chen, M.; Vit, J.-P.; Staggenborg, K.; Avalos, P.; Alkaslasi, M.; Ferraiuolo, L.; Likhite, S.; et al. Delayed Disease Onset and Extended Survival in the SOD1G93A Rat Model of Amyotrophic Lateral Sclerosis after Suppression of Mutant SOD1 in the Motor Cortex. *J. Neurosci.* **2014**, *34*, 15587−15600.
(46) Xia, J.; Chen, F.; Li, J.; Tao, N. Measurement of the Quantum Capacitance of Graphene. *Nat. Nanotechnol.* **2009**, *4*, 505−509.
(47) Ang, P. K.; Chen, W.; Wee, A. T. S.; Loh, K. P. Solution-Gated Epitaxial Graphene as PH Sensor. *J. Am. Chem. Soc.* **2008**, *130*, 14392−14393.
(48) Olson, E. J.; Ma, R.; Sun, T.; Ebrish, M. A.; Haratipour, N.; Min, K.; Aluru, N. R.; Koester, S. J. Capacitive Sensing of Intercalated H2O Molecules Using Graphene. *ACS Appl. Mater. Interfaces* **2015**, *7*, 25804−25812.
(49) Zhao, W.; Beers, D. R.; Hooten, K. G.; Sieglaff, D. H.; Zhang, A.; Kalyana-Sundaram, S.; Traini, C. M.; Halsey, W. S.; Hughes, A. M.; Sathe, G. M.; Livi, G. P.; Fan, G.-H.; Appel, S. H. Characterization of Gene Expression Phenotype in Amyotrophic Lateral Sclerosis Monocytes. *JAMA Neurol.* **2017**, *74*, 677−685.

DOI: 10.1021/acsami.8b15893
ACS Appl. Mater. Interfaces XXXX, XXX, XXX−XXX

Supporting Information

Quantum Capacitance Based Amplified Graphene Phononics for Studying Neurodegenerative Diseases

Bijentimala Keisham[1]‡, Akop Seksenyan [2,3]‡, Steven Denyer[3], Pouyan Kheirkhah[3], Gregory D. Arnone[3], Pablo Avalos[4], Abhiraj D. Bhimani[3], Clive Svendsen[4], Vikas Berry[1], Ankit I. Mehta[1,3]**

[1] Department of Chemical Engineering, University of Illinois at Chicago, Chicago IL.

[2] Chicago Medical School, Rosalind Franklin University of Medicine and Science, North Chicago, IL.

[3] Department of Neurosurgery, University of Illinois at Chicago, Chicago IL.

[4] Regenerative Medicine Institute, Cedars-Sinai Medical Center, Los Angeles, CA.

*To whom correspondence should be addressed: vikasb@uic.edu, ankitm@uic.edu

‡ B.K. and A.S. are co-first authors. These authors contributed equally to this work.

KEYWORDS. Graphene, neurodegenerative disease, Raman, ALS, phonons, detection.

S1. EXPERIMENTAL METHOD

Rat CSF Samples. Male transgenic rats were euthanized using ketamine/xylazine administered through an intraperitoneal injection. Once the animal lost response to stimuli, it was positioned prone and the head was flexed downward at approximately 45-degrees. A 25-gauge needle attached to a 1cc syringe was percutaneously introduced into the cisterna magna and approximately 50-100µl of CSF was collected. CSF was frozen on dry ice and kept at -80±10°C. Rats (ages 130+/-10 days) were defined to be "early symptomatic" when weakness was observed in locomotion and at "end point" (ages 170+/-20 days) when the animals were not able to right themselves in less than 30 seconds when placed on their side.

Graphene Production and transfer. Pretreated Cu foil (99.8%, Alfa-Aesar, annealed, uncoated) was placed inside the standard 1-inch quartz tube of the home build LP-CVD system. The reaction chamber was evacuated to ~ 1.5 mTorr and flushed with 100 sccm of H_2 (99.9999% purity, Praxair) at total pressure of 650 mTorr for 20 minutes. The temperature was then increased to 1050°C with the 10 sccm H_2 for 25 minutes. This was followed by annealing of Cu foil at 1050°C to increase the grainsize and to smoothen the surface. Subsequently, 10 sccm of CH_4 (99.999% purity, Praxair) at partial pressure of 100 mTorr with 22 sccm H_2 (~160 mTorr) was introduced into the tube for 20 minutes. Following CH_4 exposure, the reaction chamber was cooled down to room temperature in 40 minutes (25°C/minutes). Through this

CVD process, graphene was found to be synthesized on both sides of the Cu foil. PMMA solution was spin coated on one side to mask the graphene while RIE process was used on the other side to remove the graphene present there. Cu from the PMMA/graphene/Cu system was etched using a dilute HNO_3 solution (1:3), ~1 hour. Afterwards, the PMMA/Graphene system was then transferred to two consecutive DI water baths (20 minutes each) to remove any residual ions or impurities and then picked up with SiO_2/Si chip. This chip was dried overnight and subsequently placed in an acetone bath for 10 mins to remove PMMA.

Raman Spectroscopy acquisition and data analysis. The Raman spectroscopic data was obtained using WITEC Raman Alpha 300-RA, with a laser excitation wavelength of 532 nm and an exposure time of ~5 min. All the graphene samples were probed using the 100X objective. The spot size was determined using the equation:

$$Spot\ size = \frac{1.22\lambda}{NA}$$

Where λ is the wavelength of the laser and NA is the numerical aperture (0.9 for 100X objective). Also, to analyze the Raman spectra, they were all normalized to the intensity of G peak and Lorentzian curve fit was used to custom fit the 2D peaks.

The Raman spectra of the CVD grown graphene transferred on SiO_2/Si is shown in Figure S1 depicting the D, G and 2D bands, along with the optical image. The 2D/G intensity ratio was calculated to be ~2.4 and the full width at half maximum (FWHM) of 2D peak was ~29.9 cm^{-1}.[1] These values correspond to graphene monolayer produced via CVD.[2] Further, the weak D peak indicates that the CVD grown graphene is of high quality (sp^2 C orbitals).[3]

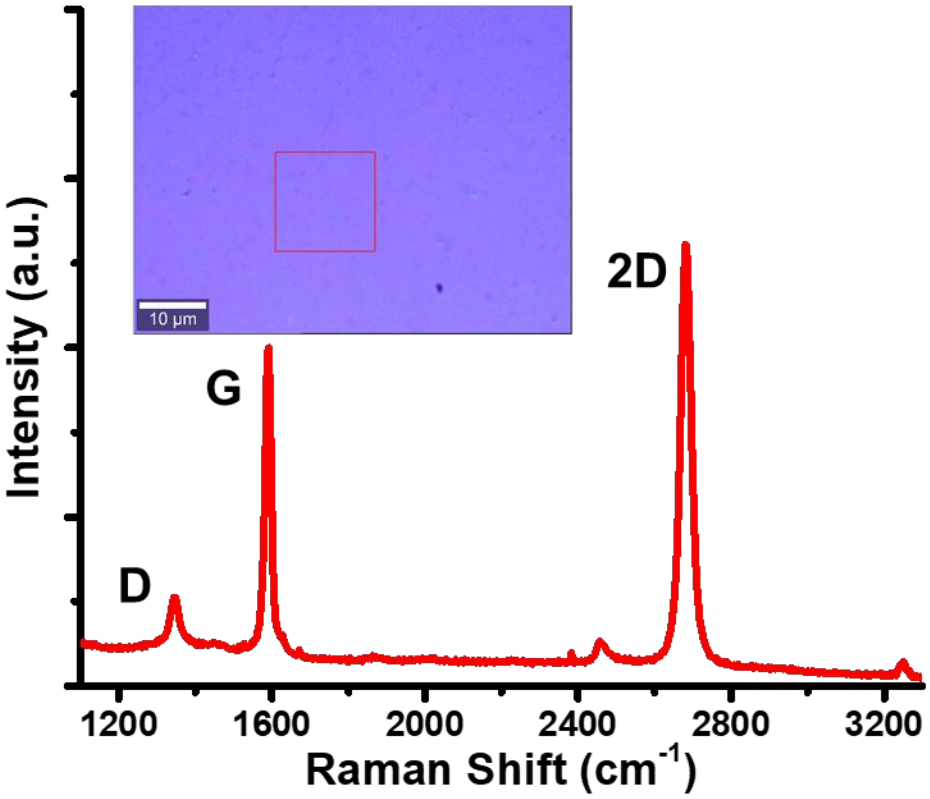

Figure S1. Raman Spectra of CVD graphene on SiO_2/Si substrate. (Inset) Optical image of graphene transferred SiO_2/Si substrate.

pH measurement. The pH of all the CSF samples were obtained using Oakton pH150.

Statistical Analysis. Student's t-test was performed throughout the study and a $p<0.05$ was used for statistical significance cutoff.

Average density estimation via quantum capacitance. The average of CSF's composite dipole moment (μ) were estimated via Hyperchem software. The composite dipole potential, originated from the charged surfaces of various proteins, lipids, nucleic acids and reactive oxygen species (present in CSF), is estimated as shown (using rectangular matrix):

$$V_{average} = \frac{\mu\rho\sin(45^o)}{4\varepsilon_o\pi}$$
$$\left(4\left\{\sum_{i=1}\left(\sqrt{(i\times d)^2+(r)^2}\right)^{-2}\right\}+8\left\{\sum_{i=1}\left(\sqrt{(i\times d\sqrt{2})^2+(r)^2}\right)^{-2}\right\}+4\left\{\sum_{i=1}\left(\sqrt{(i\times d\sqrt{5})^2+(r)^2}\right)^{-2}\right\}+\{r^{-2}\right.$$

where ε_o is vacuum permittivity (8.85 x 10^{-12} F/m), r is the distance from the molecules to the surface of graphene (~ 1 nm), $d = \sqrt{\frac{\sqrt{2}}{\rho}}$ is the distance of dipole of the charged molecules to the point of interest, i is the index (representing the distance of the dipole of the charged molecules and the point of interest), and r is vertical distance from the charged molecules to graphene surface (assumed to be 1 nm). Following this approach, the average density of the charged molecules interacting with the graphene lattice was estimated.

S2. Average dipole moment comparison for different sample groups

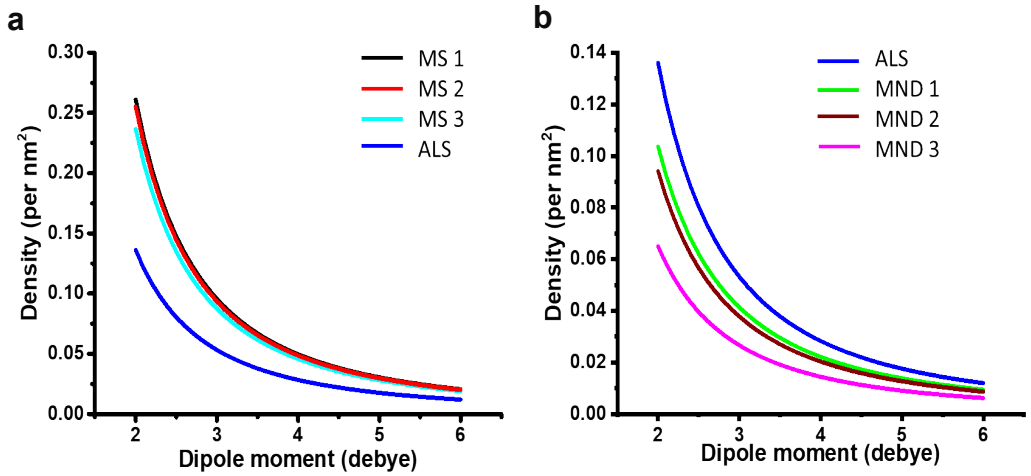

Figure S2. Calculated average induced dipole moment of human a) MS and b) MND CSF samples.

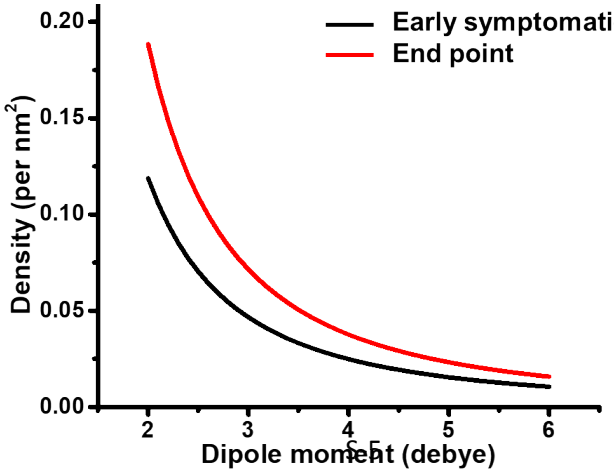

Figure S3. Calculated average induced dipole moment of CSF samples from rats at early symptomatic and end point stages.

REFERENCES:

(1) Hao, Y.; Wang, Y.; Wang, L.; Ni, Z.; Wang, Z.; Wang, R.; Koo, C. K.; Shen, Z.; Thong, J. T. L. Probing Layer Number and Stacking Order of Few-Layer Graphene by Raman Spectroscopy. *Small* **2010**, *6* (2), 195–200.

(2) Li, X.; Cai, W.; An, J.; Kim, S.; Nah, J.; Yang, D.; Piner, R.; Velamakanni, A.; Jung, I.; Tutuc, E.; Banerjee, S. K.; Colombo, L.; Ruoff, R. S. Large-Area Synthesis of High-Quality and Uniform Graphene Films on Copper Foils. *Science (80-.).* **2009**, *324* (5932), 1312–1314.

(3) Liu, L.; Ryu, S.; Tomasik, M. R.; Stolyarova, E.; Jung, N.; Hybertsen, M. S.; Steigerwald, M. L.; Brus, L. E.; Flynn, G. W. Graphene Oxidation: Thickness-Dependent Etching and Strong Chemical Doping. *Nano Lett.* **2008**, *8* (7), 1965–1970.